

Coil2Coil: Self-supervised MR image denoising using phased-array coil images

Juhyung Park, Dongwon Park, Hyeong-Geol Shin, Eun-Jung Choi, Hongjun An, Minjun Kim, Dongmyung Shin, Se Young Chun, and Jongho Lee, *Member, IEEE*

Abstract—Denoising of magnetic resonance images is beneficial in improving the quality of low signal-to-noise ratio images. Recently, denoising using deep neural networks has demonstrated promising results. Most of these networks, however, utilize supervised learning, which requires large training images of noise-corrupted and clean image pairs. Obtaining training images, particularly clean images, is expensive and time-consuming. Hence, methods such as Noise2Noise (N2N) that require only pairs of noise-corrupted images have been developed to reduce the burden of obtaining training datasets. In this study, we propose a new self-supervised denoising method, Coil2Coil (C2C), that does not require the acquisition of clean images or paired noise-corrupted images for training. Instead, the method utilizes multichannel data from phased-array coils to generate training images. First, it divides and combines multichannel coil images into two images, one for input and the other for label. Then, they are processed to impose noise independence and sensitivity normalization such that they can be used for the training images of N2N. For inference, the method inputs a coil-combined image (e.g., DICOM image), enabling a wide application of the method. When evaluated using synthetic noise-added images, C2C shows the best performance against several self-supervised methods, reporting comparable outcomes to supervised methods. When testing the DICOM images, C2C successfully denoised real noise without showing structure-dependent residuals in the error maps. Because of the significant advantage of not requiring additional scans for clean or paired images, the method can be easily utilized for various clinical applications.

Index Terms—MRI, Self-supervised learning, Noise2Noise, Real image denoising.

I. INTRODUCTION

Magnetic resonance imaging (MRI) is a powerful modality for *in-vivo* imaging. Magnetic resonance (MR) images have a finite signal-to-noise ratio (SNR) [1] and often suffer from SNR deficiency, hampering accurate diagnosis or proper processing of the images. Therefore, enhancing image SNR has long been an important research topic in MR image processing. One popular approach to improving SNR is using denoising

algorithms [2], which are designed as post-processing tools and can be applied to existing images. Traditionally, algorithms such as filtering-based methods [3-5] and low-rank-based methods [6, 7] have been developed.

Recently in the computer vision field, deep learning-based denoising methods have been widely investigated [8, 9]. When applying supervised learning, a denoising network is developed by training the network using pairs of images, consisting of a noise-corrupted image and a clean image [10]. In most cases, however, obtaining a clean image is expensive or sometimes impossible. Hence, another method, Noise2Noise (N2N) [11], that can train a network without clean images is proposed. This method utilizes pairs of noisy images that have the same origin but are corrupted by independent noise, relaxing the condition of requiring clean images in the supervised learning. Despite this advantage, however, N2N still has limited applicability due to the necessity of two noise-corrupted images [12]. To overcome this limitation, methods have been suggested using self-supervised learning, requiring only one noisy image at the cost of performance degradation [13-16].

In MRI, deep learning has been successfully applied in various steps of processing [17-20], including denoising [21-26], and has been demonstrated to outperform conventional approaches. As was the case for non-MRI denoising, MRI denoising methods were developed largely using supervised learning, requiring clean images [21-26]. More recently, studies have proposed self-supervised denoising methods by utilizing redundancy in a specific MR sequence (e.g., redundancy of b-value domain in diffusion-weighted imaging (DWI) [27] and temporal domain in dynamic MR imaging [28]). Although these methods are free from the constraint of obtaining clean images, the usability of these methods is limited to specific MR acquisitions (i.e., DWI and dynamic MR). As a more general self-supervised method, a modified N2N method, which is referred to as N2N-CS, was proposed by incorporating compressed sensing [11]. In this method, a paired image was created by two independently undersampled k-space data that were reconstructed by compressed sensing. Because of the two

This research was supported by the National Research Foundation of Korea, NRF-2022R1A4A1030579, NRF-2019M3C7A1031994, NRF-2021M3E5D2A01024795, RadiSen Co. Ltd, Creative-Pioneering Researchers Program, Institute of Engineering Research, Institute of New Media and Communications at Seoul National University.

*Corresponding author: J. Lee (jonghoyi@snu.ac.kr).

J. Park, E.-J. Choi, H. An, M. Kim, S. Y. Chun and J. Lee are with the Department of Electrical and Computer Engineering, Seoul National University, Republic of Korea. (e-mail: jack0878@snu.ac.kr; ej_ejchoi@snu.ac.kr; plynt@snu.ac.kr; minjoony@snu.ac.kr; sychun@snu.ac.kr; jonghoyi@snu.ac.kr).

D. Park is with the Department of Electrical Engineering, Ulsan National Institute of Science and Technology, Ulsan, Republic of Korea (e-mail: dong1@unist.ac.kr).

H.-G. Shin is with the Department of Radiology, Johns Hopkins University School of Medicine, Baltimore, MD and F.M. Kirby Research Center for Functional Brain Imaging, Kennedy Krieger Institute, Baltimore, MD (e-mail: sin4109@gmail.com).

D. Shin is with the AI Engineering Division, RadiSen Co. Ltd., Seoul, Republic of Korea (e-mail: shinsae11@gmail.com).

different undersampling patterns and complex nonlinear reconstruction, the clean image might not be perfectly matched, limiting denoising performance.

In this study, we propose a new self-supervised method, which does not require clean images nor the acquisition of paired noise-corrupted images. The method generates a pair of noise-corrupted images from phased-array coil data and utilizes the pair for network training, requiring only multi-channel data. For inference, the method can input a channel-combined image (e.g., DICOM image), enabling a wide application of the method. Denoising experiments were performed with synthetic noise-added images and DICOM images, evaluating the performances of the proposed method. This new method is referred to as Coil2Coil (C2C), hereafter. The source code of C2C is available on Github (<https://github.com/SNU-LIST/Coil2Coil>).

II. METHODS

A. Noise2Noise

In N2N, a denoising network is trained with pairs of noise-corrupted images, with one image as an input and the other image as a label, learning the characteristics of noise between the two images for denoising [11]. The method requires the following three conditions: (1) The paired images have independent noise. (2) They have the same noise-free image. (3) The expectation of the noise is zero. Note that the power of the noise in the paired images does not have to be the same (see Discussion). When training a denoising network, L2 loss between the output and label is used. Despite the advantage of

not requiring noise-free images, the method still has limited applicability due to the requirement for paired noise-corrupted images. Therefore, subsequent studies have proposed denoising methods using a single noise-corrupted image by masking out some pixels of the input image and utilizing the masked pixels as a label [13-15]. Depending on a mask generation scheme, the method is referred to as Noise2Void (N2V: when the masked pixels are randomly chosen [13]), or Noise2Self (N2Se: when a masking scheme is suggested based on the independence of the input image and label pixels [14]), or Noise2Same (N2Sa: when self-similarity loss between input and denoised images is utilized [15]). All of these methods, however, showed performance degradation when compared to N2N. As mentioned earlier, N2N-CS was proposed in MRI, reporting similar degradation [11].

B. Coil2Coil: generation of input and label images

In C2C, paired noise-corrupted images that satisfy the three conditions of N2N are generated from the combination of phased-array coil data (Fig. 1). Then, the pairs are applied to train a denoising network as described in N2N.

When a phased-array coil is utilized to acquire an MR image ($x \in \mathbb{C}^2$), an individual channel image ($y_i \in \mathbb{C}^2$) of i^{th} channel ($i \in M = [1 \dots m]$) can be formulated as $y_i = s_i x + n_i$, where $s_i \in \mathbb{C}^2$ is the coil sensitivity and $n_i (= n_{ri} + in_{ii})$ is the noise of i^{th} channel, modeled as zero mean Gaussian with the standard deviation of σ_i for both real and imaginary axes ($n_{ri} \in \mathbb{R}^2$ and $n_{ii} \in \mathbb{R}^2$). The matrix multiplication (or division) hereafter indicates Hadamard multiplication (or

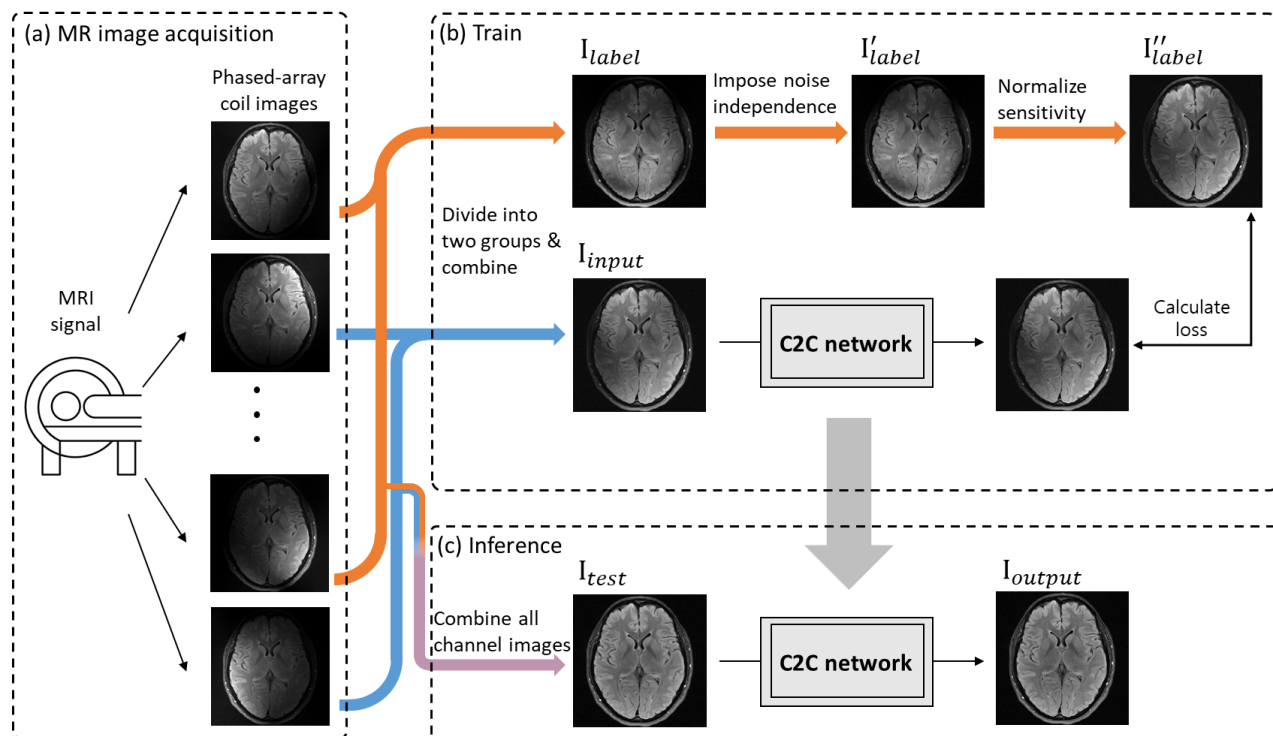


Fig. 1. Overview of Coil2Coil (C2C). (a) When using a phased-array coil, multiple channel images are acquired. In C2C, these images are divided into two groups and combined to generate I_{input} and I_{label} . Then, I_{label} is processed for noise independence and normalized for coil sensitivity in order to satisfy the conditions of N2N. Finally, this processed image (I''_{label}) paired with I_{input} is utilized for the training of a denoising neural network. (c) For inference, all channel images are combined (e.g., DICOM image) and used as an input for the network, creating a denoised image.

division). In C2C, these channel images are grouped into two sets such that each set generates either an input (I_{input}) or label (I_{label}) image:

$$I_{input} = |\sum_j s_j^H y_j| \quad (\text{Eq. 1})$$

$$I_{label} = |\sum_k s_k^H y_k|, \quad (\text{Eq. 2})$$

where half of the channels are in j and the other half in k , and s_i^H is the hermitian of s_i . We assume that the two images cover all imaging volumes because most of the individual coils have relatively large volume coverage and are mutually coupled (see Fig. 1a).

These two images, however, have different coil sensitivity weighting (see I_{input} and I_{label} in Fig. 1b) and may have noise correlation (e.g., mutual inductance between channels) [29]. Therefore, they need to be further processed to satisfy the three conditions of N2N. In order to impose the independence of noise between the two images, a generalized least-square solution is applied, resulting in the following modification in the label image [30] (see Appendix):

$$I'_{label} = \alpha I_{input} + \beta I_{label} \quad (\text{Eq. 3})$$

$$\text{with } \alpha = \frac{-\sigma_{jK}^2}{\sigma_j^2 \sigma_K^2 - (\sigma_{jK}^2)^2}, \text{ and } \beta = \frac{\sigma_j^2}{\sigma_j^2 \sigma_K^2 - (\sigma_{jK}^2)^2},$$

where σ_j^2 , σ_K^2 , and σ_{jK}^2 are matrices ($\in \mathbb{R}^2$) calculated as $\text{var}(|\sum_j s_j^H y_j|)$, $\text{var}(|\sum_k s_k^H y_k|)$, and $\text{cov}(|\sum_j s_j^H y_j|, |\sum_k s_k^H y_k|)$, respectively. In these equations, all operations are voxel-wise operations. As a result, I_{label} is modified to I'_{label} , and thereby the noise covariance between I_{input} and I'_{label} becomes zero.

To impose the requirement of the same noise-free image, the coil sensitivity of I'_{label} (i.e., $S'_K = \alpha |\sum_k s_k^H| + \beta |\sum_j s_j^H|$) is modified to match that of I_{input} (i.e., $S_j = |\sum_j s_j^H|$) by multiplying the sensitivity ratio (S_j/S'_K) to I'_{label} in each voxel, generating a final image ($I''_{label} = (S_j/S'_K) \cdot I'_{label}$). Since multiplying a coefficient is a linear process, the first condition of noise independence still holds after the processing.

The third condition of zero-mean noise in N2N is valid, assuming that the combined images have reasonably high SNR such that the noise characteristics within the image can be considered as Gaussian with zero mean [31].

For inference, the images of all channels are combined to generate an input image (i.e., $I_{test} = |\sum_l s_l^H y_l|$; Fig. 1c). Additional options exist for the input images (see Discussion). Finally, scanner-generated DICOM images are also evaluated.

For the training of a denoising network, the L2 loss is utilized as follows:

$$\text{loss} = |S'_K f_\theta(I_{input}) - S_j I'_{label}|_2^2, \quad (\text{Eq. 4})$$

where f_θ is the neural network. Note that the scaled version of I'_{label} is used instead of I''_{label} to avoid division. This loss function is calculated within a brain mask.

C. Deep neural network

For the structure of the neural network, DnCNN [32] was tested. It consists of a total of 18 convolutional layers. The first convolutional layer is followed by a leaky rectified linear unit (ReLU; alpha = 0.1) [33], and then 16 convolutional layers are followed by batch normalization [34] and leaky ReLU (alpha = 0.1) each. The last convolutional layer generates an output, and a skip connection is applied to the output from the first layer to the end layer of the network [35]. This original structure was maintained except for the convolutional kernel size, which was modified from 3×3 to 5×5 for an increased network capacity.

The initial weights of the network parameters were set by the Xavier initializer [36]. The learning rate was $1e-4$, and a decaying factor of 0.87 was applied for each epoch. For an optimizer, an Adam optimizer was utilized [37]. The batch size was 8. The training process was stopped after 100 epochs. For each epoch, the channel combinations for the input and label images were randomly determined for generalization.

The network training was performed on a GPU workstation (TITAN Xp GPU with Intel i7-7800X CPU at 3.50GHz) using PyTorch [38]. The total training time was approximately 78 hours.

D. Datasets

For the training and test, the NYU fastMRI brain train and test datasets, containing T1-weighted, T2-weighted, and fluid attenuation inversion recovery (FLAIR) images from 1.5 T and 3 T were utilized [39]. The number of channels ranged from 4 to 20.

As a preprocessing step, each subject was normalized by the mean and standard deviation. The upper three slices were excluded because they were usually background. A total of 34341 and 8284 slices were utilized as the training and test datasets, respectively. The sensitivity map of each channel image was calculated using ESPiRiT [40]. The brain mask was obtained using a brain extraction tool [41]. All preprocessing steps were performed using MATLAB (MATLAB2020a, MathWorks Inc., Natick, MA, USA).

E. Denoising of synthetic noise added images

To quantitatively analyze the performance of C2C, denoising experiments were performed by adding synthetic noise to the data. A virtual true image, \hat{x} , which was considered as a clean image in this synthetic noise experiment, was calculated by combining all channel images ($= \sum_l s_l^H y_l$). To simulate the synthetic channel image, \hat{y}_i ($i \in M = [1 \dots m]$), \hat{x} was multiplied by the coil sensitivity, s_i , and was then corrupted by complex noise ($n_{ri} + in_{ii}$; each axis with zero-mean Gaussian noise with the standard deviation of $|\overline{s_i \hat{x}}| \sqrt{2}^{-1} \sigma$, where $|\overline{s_i \hat{x}}|$ was the mean of the voxels within the brain mask and σ was the noise level set to be 1.0 as default). The noise correlation between two channels was randomly chosen from 0.0 to 0.2.

Finally, these data were processed using C2C and utilized for training. When evaluating the trained network, three noise levels, σ of 0.5, 1.0, and 1.5, were tested.

The performance of C2C was compared to that of several denoising methods. As supervised methods, Noise2Clean (N2CL) [10], which used a noise-corrupted image as an input and a clean image as a label, and N2N were tested. For self-supervised methods, N2V, N2Se, N2Sa, N2N-CS, and a self-supervised denoising network (SSDN) by Laine, et al. [42] were tested. These methods utilized all channel combined images (=

$|\sum_l s_l^H \hat{y}_l|$) for training using the same network structure as C2C except for SSDN. In order to evaluate the denoising performance, the quantitative metrics, peak signal-to-noise ratio (pSNR) and structural similarity index (SSIM), were measured between the denoised image and clean image within the brain mask. The means and standard deviation of the quantitative metrics were reported for all slices of the test dataset. A paired t -test was performed for the quantitative metrics between C2C and the self-supervised methods. For statistical significance, the p-value threshold was set to be 0.05.

Synthetic noise denoising

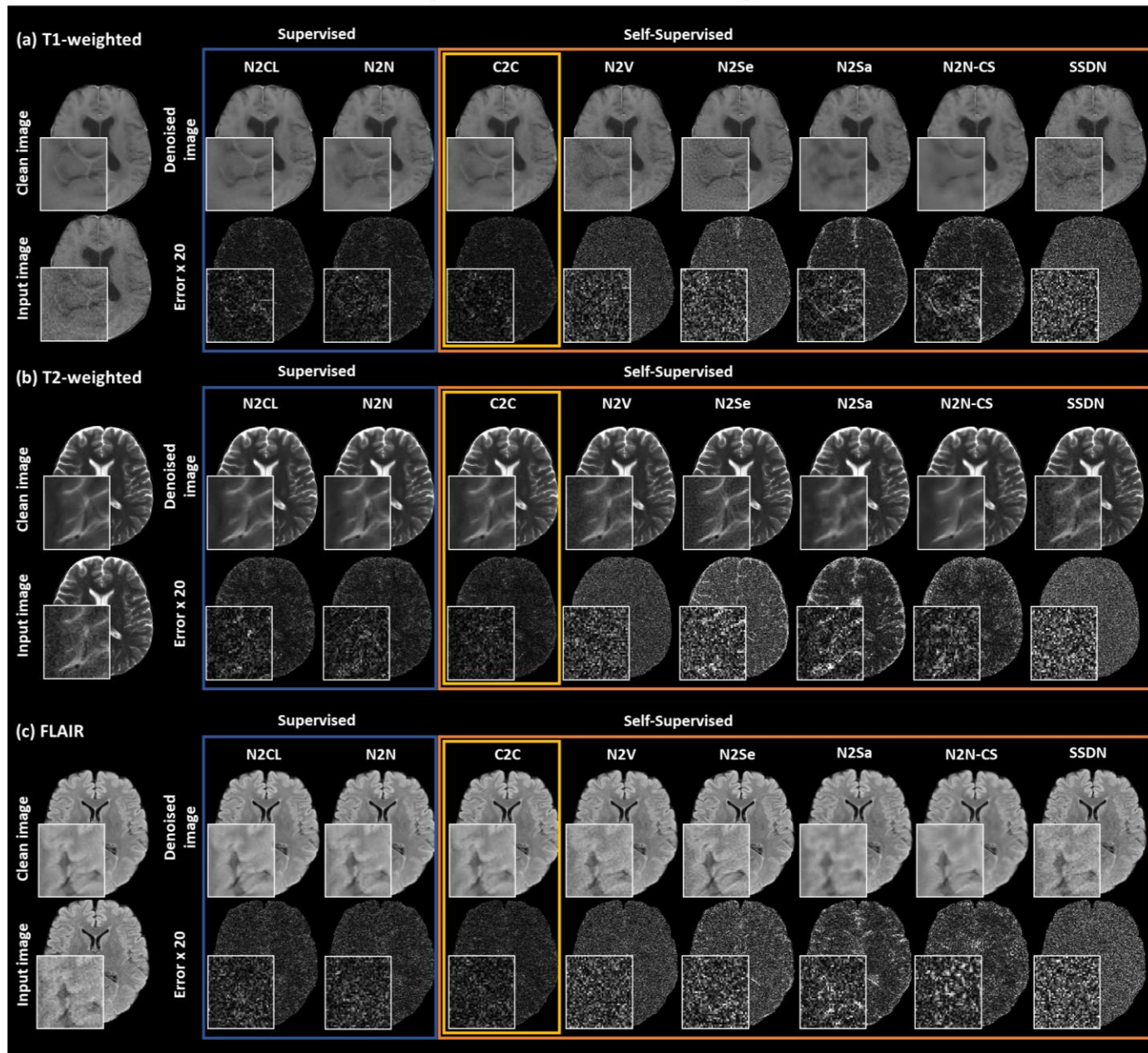


Fig. 2. Denoised images of the synthetic noise denoising experiment. (a) T1-weighted images: The clean image and noise-corrupted input image are shown in the first column. Denoised images using the supervised learning (N2CL and N2N; blue boxes) and self-supervised learning (C2C, N2V, N2Se, N2Sa, N2N-CS, and SSDN; orange boxes) are shown along with the error maps at the scale of error $\times 20$. The results of T2-weighted images (b) and FLAIR images (c) are presented in the same format. The C2C results show superior images to those of the self-supervised learning methods, providing comparable outcomes to the supervised learning methods that require additional acquisition of paired images for training.

TABLE I
QUANTITATIVE RESULTS FOR THE SYNTHETIC NOISE DENOISING EXPERIMENT

		pSNR	SSIM
Supervised Learning	N2CL	39.56 ± 2.71	0.978 ± 0.010
	N2N	39.18 ± 2.96	0.968 ± 0.017
		C2C	38.97 ± 2.91
		N2V	$35.09 \pm 3.48^*$
Self-supervised Learning	N2Se	$35.38 \pm 3.36^*$	$0.933 \pm 0.042^*$
	N2Sa	$36.34 \pm 2.29^*$	$0.951 \pm 0.016^*$
	N2N-CS	$37.10 \pm 2.66^*$	$0.955 \pm 0.019^*$
	SSDN	$37.08 \pm 3.46^*$	$0.926 \pm 0.046^*$

pSNR and SSIM of the denoising methods for the synthetic noise denoising experiment (* denotes a statistically significant difference between self-supervised learning denoising method and C2C).

Ablation studies were performed to estimate the effects of the two processing steps of C2C (i.e., noise independence and sensitivity normalization). To assess the noise independence processing, the performance of C2C was evaluated with and without imposing the condition by replacing the label I'_{label} with I_{label} . Then, a new network, C2C_{dependent}, was trained and the results were compared with those of C2C when the maximum noise correlation was varied from 0.0 to 0.5. To explore the effects of the sensitivity normalization, the performance of C2C was evaluated with and without the normalization. A new network, C2C_{unnormalized}, was trained and the results were compared to those of C2C.

F. Denoising of real world images

Experiments were performed to denoise real world images (i.e., DICOM images directly from scanners). The network was trained using the same procedure as in the synthetic noise experiment but with no additional noise. For test, the NYU fastMRI brain DICOM dataset, containing T1-weighted, T2-weighted, and FLAIR images, was utilized [39]. For comparison, the self-supervised methods, N2V, N2Se, N2Sa, N2N-CS, and SSDN, were trained and tested using the same datasets.

III. RESULTS

The results of the synthetic noise denoising experiment are shown in Fig. 2. Our method (C2C) successfully denoised the synthetic noise, generating high-quality images similar to the clean images in all three contrasts (see the images in the yellow boxes and compared them to the clean images in the first column). When compared to the results of the supervised learning methods (blue boxes), the C2C images reveal similar image qualities that can be confirmed by the error $\times 20$ images. On the other hand, the outputs of the other self-supervised learning methods (orange boxes) show performance degradations that are manifested in both output and error images (e.g., blurring in the N2Sa and N2N-CS images, persistent noise in the N2V, N2Se, and SSDN images). When analyzed quantitatively, C2C reports the highest pSNR (38.97 ± 2.91 ; $p < 0.001$) and SSIM (0.968 ± 0.017 ; $p < 0.001$) among the self-supervised learning methods, confirming the visual inspection results (Table 1). Furthermore, the performance of

C2C is comparable to those of the supervised learning methods despite the self-supervised learning nature of C2C.

When the denoising methods were evaluated by varying the noise level σ from 0.5 to 1.5, the results were consistent (Fig. 3). Our C2C outperformed the other self-supervised denoising methods while reporting a comparable performance to the

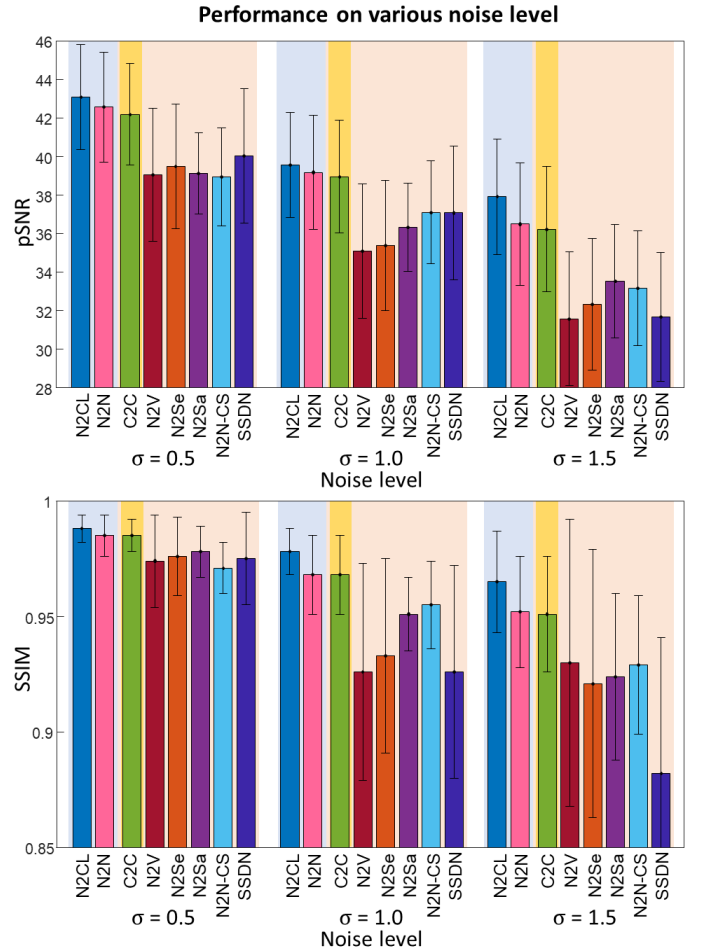


Fig. 3. pSNR and SSIM of the supervised (blue background) and self-supervised learning methods (orange background; C2C in yellow background) for the synthetic noise denoising experiments in various noise levels ($\sigma = 0.5, 1.0, \text{ and } 1.5$). The quantitative metrics suggest a consistent denoising performance of C2C for the different levels of noise, providing comparable outcomes to the supervised learning methods.

Performance of C2C with and without imposing noise independence

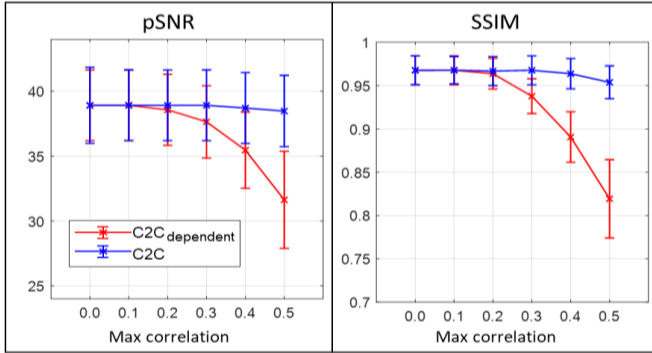


Fig. 4. pSNR and SSIM of C2C with and without applying the noise independence processing. The results demonstrate that the performance degrades for correlated noises when the process is not applied.

supervised methods, demonstrating the robustness of C2C for noise levels.

The ablation study of evaluating the noise independence processing step suggests that the step successfully improves the performance when noise correlation between the input and label images exists (Fig. 4). When C2C was trained without the sensitivity normalization step (C2C_{unnormalize}), it failed to denoise the test image (pSNR: 24.72 ± 4.01 ; SSIM: 0.712 ± 0.060).

When the real world images (i.e., DICOM) are processed for denoising (Fig. 5), C2C successfully denoised the images, showing little or no structure-dependent error (yellow box). Similar to the synthetic noise experiment, the N2Sa and N2N-CS images show blurring while N2V, N2Se, and SSDN yield less denoised images. No result of the supervised learning methods are available because the dataset contains no clean image nor paired noise-corrupted image.

Real world image denoising

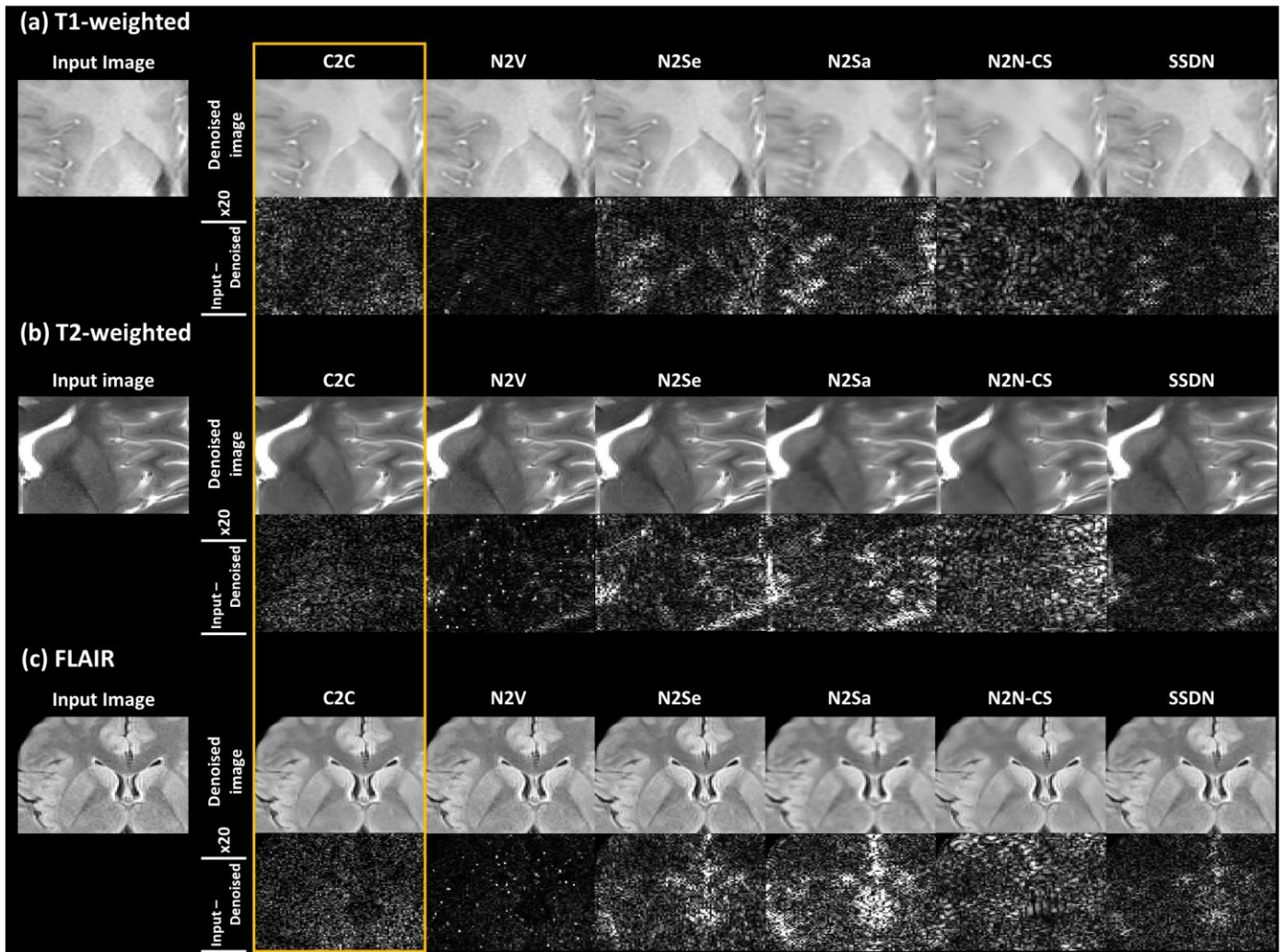


Fig. 5. Denoising results of the real world DICOM images using the self-supervised methods. (a) T1-weighted image: The input image contains a noticeable level of noise whereas the denoised images using C2C, N2V, N2Se, N2Sa, N2N-CS, and SSDN show improved results. The differences are shown below the denoised images. The results of T2-weighted images (b) and FLAIR images (c) are also displayed. In all results, C2C images are superior to the other results, showing little or no structure in the difference maps.

IV. DISCUSSION

In this study, we proposed a novel self-supervised MRI denoising framework, C2C, which generated a pair of noise-corrupted images from phased-array coil data to train a deep neural network. The paired images were modified to satisfy the conditions of N2N, enabling network training using N2N. C2C showed the best performance among the self-supervised methods, while reaching comparable outcomes to the supervised methods. The method successfully denoised the real world images, demonstrating wide applicability.

In previous studies, a few self-supervised denoising methods were proposed to utilize redundancy in data from specific sequences (e.g., DWI [27] and dynamic MR [28]), limiting applications of the methods. On the other hand, C2C is not limited to a specific sequence and, therefore, can be utilized more generally. Furthermore, it can be extended to train complex images in order to denoise both magnitude and phase images.

In C2C training, the noise level of the paired images can be different depending on the combinations of channel images or the scaling process. This does not violate the conditions of N2N because the conditions do not require the same level of noise in the paired images as demonstrated in [11].

The number of the network parameters in our DnCNN was $1.64e+6$, which was larger than that of SSDN ($1.27e+6$). When we tested DnCNN with a decreased number of the parameters ($0.59e+6$) by reducing the kernel size from 5×5 to 3×3 , our method still outperformed SSDN (pSNR: 38.25 ± 2.45 vs. pSNR: 37.08 ± 3.46 ; SSIM: 0.958 ± 0.022 vs. 0.926 ± 0.046 ; $p < 0.001$).

In MRI, noise originates from multiple sources such as sample (e.g., brain) and hardware (e.g., receiver chain) [43]. Since sample noise is common in all channels, we expect our method removes noise from the receiver chain (e.g., coil, preamplifier, etc.), which may or may not be dominant depending on the size of the coil relative to the sample [44]. Despite this limitation, the real world data results indicate that the method may perform beyond the receiver chain noise removal potentially because of the nature of a denoising neural network that inputs multiple voxels (5×5 in our case), utilizing information from neighboring voxels for denoising.

While developing C2C, we also tested U-net [45] as an alternative network structure. The results were almost the same, except for slight performance degradation when compared to DnCNN.

As another option for inference, we tested an approach that combined all channel images into two and then inferenced the two images, generating two C2C denoised images. When these images were averaged as the final output, the performances were slightly worse than the current approach of combining all channels and then inferencing (pSNR dropped from 38.97 ± 2.91 to 38.10 ± 2.88 and SSIM reduced from 0.968 ± 0.017 to 0.962 ± 0.017).

The proposed method is based on the assumption that the paired images generated from different combinations of the channels sufficiently cover the imaging volume which may not

be valid when using a coil with a small number of channels or channels with limited coverages, potentially degrading the performance of our method.

To process an image of an unseen contrast or data of an untrained coil, transfer learning with a small number of training data can be performed.

Our method utilized the redundancy of phased-array coil data. It may be combined with additional redundancy (e.g., multi-echo data, multi-contrast data) to provide an further improvement in denoising performance.

V. CONCLUSION

In this work, a novel self-supervised denoising method, C2C, was developed for MRI. Compared to supervised learning, the method does not require noise-free images nor multiple data acquisition, making it easy to train and utilize the network. Furthermore, the network can input various contrast DICOM images, demonstrating its wide applicability for future practices.

APPENDIX

A linear equation can be written as follows:

$$y = Ax + n \quad (\text{Eq. 5})$$

with $\text{var}(y) = \Sigma$,

where $y (\in \mathbb{R})$ is an N vector of observation, $A (\in \mathbb{R}^2)$ is an $N \times M$ matrix, $x (\in \mathbb{R})$ is an M vector of data, $n (\in \mathbb{R})$ is an N vector of noise, and $\Sigma (\in \mathbb{R}^2)$ is a noise covariance matrix of y . Since a covariance matrix is symmetric and positive semi-definite, Σ can be decomposed into LL^T , where L is a lower triangular matrix with positive diagonal entries [46].

We can impose independence among the noise vectors by multiplying L^{-1} to Eq. 5 [30]:

$$L^{-1}y = L^{-1}Ax + L^{-1}n. \quad (\text{Eq. 6})$$

Then, the new noise covariance matrix ($\text{var}(L^{-1}y)$) becomes an identity matrix as shown below.

$$\text{var}(L^{-1}y) = L^{-1}\text{var}(y)(L^{-1})^T = L^{-1}(LL^T)(L^{-1})^T = I. \quad (\text{Eq. 7})$$

In the case of $N = 2$, we can express L^{-1} in terms of the components of Σ :

$$\Sigma = \begin{bmatrix} \sigma_j^2 & \sigma_{jk}^2 \\ \sigma_{jk}^2 & \sigma_k^2 \end{bmatrix} = LL^T = \begin{bmatrix} L_{11} & 0 \\ L_{21} & L_{22} \end{bmatrix} \begin{bmatrix} L_{11} & L_{21} \\ 0 & L_{22} \end{bmatrix}. \quad (\text{Eq. 8})$$

where σ_j^2 , σ_{jk}^2 , and σ_k^2 are the noise variances and covariance of the observations. Then we have

$$L^{-1} = \frac{1}{\sqrt{\sigma_j^2}} \begin{pmatrix} 1 & 0 \\ \frac{-\sigma_{jk}^2}{\sqrt{\sigma_j^2 \sigma_k^2 - (\sigma_{jk}^2)^2}} & \frac{\sigma_j^2}{\sqrt{\sigma_j^2 \sigma_k^2 - (\sigma_{jk}^2)^2}} \end{pmatrix}. \quad (\text{Eq. 9})$$

In C2C, we have the two observations ($I_{input} (= |\sum_j s_j^H y_j|)$ $I_{label} (= |\sum_k s_k^H y_k|)^T$) and the noise variances and covariance (σ_j^2 , σ_k^2 , and σ_k^2) for each voxel. Hence, we can impose noise independence by applying the inverse lower triangular matrix as shown above. To keep I_{input} the same, $\sqrt{\sigma_j^2}$ is multiplied, generating the final formula in Eq. 3.

REFERENCES

- [1] A. Macovski, "Noise in MRI," *Magn. Reson. Med.*, vol. 36, no. 3, pp. 494-497, Sep. 1996.
- [2] J. Mohan, V. Krishnaveni, and Y. Guo, "A survey on the magnetic resonance image denoising methods," *Biomed. Signal Process. Control*, vol. 9, pp. 56-69, Jan. 2014.
- [3] K. Dabov, A. Foi, V. Katkovnik, and K. Egiazarian, "Image denoising by sparse 3-D transform-domain collaborative filtering," *IEEE Trans. Imag. Proc.*, vol. 16, no. 8, pp. 2080-2095, Jul. 2007.
- [4] A. Buades, B. Coll, and J.-M. Morel, "A non-local algorithm for image denoising," in *Proc. IEEE Int. Conf. Comput. Vis. Pattern Recognit.*, vol. 2, pp. 60-65, Jul. 2005.
- [5] T. Loupas, W. McDicken, and P. L. Allan, "An adaptive weighted median filter for speckle suppression in medical ultrasonic images," *IEEE Trans. Circuit. Sys.*, vol. 36, no. 1, pp. 129-135, Jan. 1989.
- [6] S. V. M. Sagheer and S. N. George, "Ultrasound image despeckling using low rank matrix approximation approach," *Biomed. Signal Process. Control*, vol. 38, pp. 236-249, Sep. 2017.
- [7] H. S. Khaleel, S. V. M. Sagheer, M. Baburaj, and S. N. George, "Denoising of Rician corrupted 3D magnetic resonance images using tensor-SVD," *Biomed. Signal Process. Control*, vol. 44, pp. 82-95, Jul. 2018.
- [8] C. Tian, L. Fei, W. Zheng, Y. Xu, W. Zuo, and C.-W. Lin, "Deep learning on image denoising: An overview," *Neural Networks*, vol. 131, pp. 251-275, Nov. 2020.
- [9] H. C. Burger, C. J. Schuler, and S. Harmeling, "Image denoising: Can plain neural networks compete with BM3D?," in *Proc. IEEE Int. Conf. Comput. Vis. Pattern Recognit.*, vol. 2, pp. 2392-2399, Jun. 2012.
- [10] V. Jain and S. Seung, "Natural image denoising with convolutional networks," in *Proc. Adv. Neural Inf. Process. Syst.*, vol. 21, pp. 769-776, Dec. 2008.
- [11] J. Lehtinen et al., "Noise2Noise: Learning image restoration without clean data," in *Proc. Int. Conf. Mach. Learn.*, pp. 2965-2974, Jul. 2018.
- [12] A. A. Hendriksen, D. M. Pelt, and K. J. Batenburg, "Noise2Inverse: Self-supervised deep convolutional denoising for tomography," *IEEE Trans. Comput. Imag.*, vol. 6, pp. 1320-1335, Aug. 2020.
- [13] A. Krull, T.-O. Buchholz, and F. Jug, "Noise2Void-learning denoising from single noisy images," in *Proc. IEEE Int. Conf. Comput. Vis. Pattern Recognit.*, pp. 2129-2137, Jun. 2019.
- [14] J. Batson and L. Royer, "Noise2Self: Blind denoising by self-supervision," in *Proc. Int. Conf. Mach. Learn.*, pp. 524-533, Jun. 2019.
- [15] Y. Xie, Z. Wang, and S. Ji, "Noise2Same: Optimizing a self-supervised bound for image denoising," in *Proc. Adv. Neural Inf. Process. Syst.*, vol. 33, pp. 20320-20330, Dec. 2020.
- [16] M. Zhussip, S. Soltanayev, and S. Y. Chun, "Extending Stein's unbiased risk estimator to train deep denoisers with correlated pairs of noisy images," in *Proc. Adv. Neural Inf. Process. Syst.*, vol. 32, pp. 1465-1475, Dec. 2019.
- [17] A. S. Lundervold and A. Lundervold, "An overview of deep learning in medical imaging focusing on MRI," *Zeitschrift Für Medizinische Physik*, vol. 29, pp. 102-127, May. 2019.
- [18] M. Akçakaya, S. Moeller, S. Weingärtner, and K. Uğurbil, "Scan-specific robust artificial-neural-networks for k-space interpolation (RAKI) reconstruction: Database-free deep learning for fast imaging," *Magn. Reson. Med.*, vol. 81, pp. 439-453, Sep. 2019.
- [19] J. Yoon et al., "Quantitative susceptibility mapping using deep neural network: QSMnet," *Neuroimage*, vol. 179, pp. 199-206, Oct. 2018.
- [20] D. Shin et al., "Deep reinforcement learning-designed radiofrequency waveform in MRI," *Nature Mach. Intel.*, vol. 3, no. 11, pp. 985-994, Nov. 2021.
- [21] L. Gondara, "Medical image denoising using convolutional denoising autoencoders," in *Proc. Int. Conf. data mining workshops*, pp. 241-246, Dec. 2016.
- [22] D. Jiang, W. Dou, L. Vosters, X. Xu, Y. Sun, and T. Tan, "Denoising of 3D magnetic resonance images with multi-channel residual learning of convolutional neural network," *Jap. J. Radiol.*, vol. 36, no. 9, pp. 566-574, Jul. 2018.
- [23] X. Xu et al., "Noise Estimation-based Method for MRI Denoising with Discriminative Perceptual Architecture," in *Proc. Int. Conf. Internet of Things (iThings) IEEE Green Comput. and Commun. (GreenCom) and IEEE Cyber Phys. Soc. Comput. (CPSCom) and IEEE Smart Data (SmartData) IEEE Congr. Cybermatics (Cybermatics)*, pp. 469-473, Nov. 2020.
- [24] J. V. Manjón and P. Coupe, "MRI denoising using deep learning," in *Proc. Int. Patch Based Tech. Med. Imag.*, pp. 12-19, Sep. 2018.
- [25] S. Li, J. Zhou, D. Liang, and Q. Liu, "MRI denoising using progressively distribution-based neural network," *Magn. Reson. Med.*, vol. 71, pp. 55-68, Sep. 2020.
- [26] M. Kidoh et al., "Deep learning based noise reduction for brain MR imaging: tests on phantoms and healthy volunteers," *Magn. Reson. Med. Sci.*, vol. 19, no. 3, pp. 195, Sep. 2020.
- [27] S. Fadnavis, J. Batson, and E. Garyfallidis, "Patch2Self: denoising diffusion MRI with self-supervised learning," in *Proc. Adv. Neural Inf. Process. Syst.*, vol. 33, pp. 1-11, Dec. 2020.
- [28] J. Xu and E. Adalsteinsson, "Deformed2Self: Self-Supervised Denoising for Dynamic Medical Imaging," in *Proc. Int. Conf. Med. Image Comput. Comput.-Assist. Intervent.*, vol. 10902, pp. 25-35, Sep. 2021.
- [29] C. E. Hayes and P. B. Roemer, "Noise correlations in data simultaneously acquired from multiple surface coil arrays," *Magn. Reson. Med.*, vol. 16, no. 2, pp. 181-191, Nov. 1990.
- [30] A. C. Aitken, "IV.—On least squares and linear combination of observations," in *Proc. R. Soc. Edinb.*, vol. 55, pp. 42-48, Sep. 1936.
- [31] R. M. Henkelman, "Measurement of signal intensities in the presence of noise in MR images," *Med. Phys.*, vol. 12, no. 2, pp. 232-233, Mar. 1985.
- [32] K. Zhang, W. Zuo, Y. Chen, D. Meng, and L. Zhang, "Beyond a gaussian denoiser: Residual learning of deep cnn for image denoising," *IEEE trans. Imag. Proc.*, vol. 26, no. 7, pp. 3142-3155, Feb. 2017.
- [33] A. L. Maas, A. Y. Hannun, and A. Y. Ng, "Rectifier nonlinearities improve neural network acoustic models," in *Proc. Int. Conf. Mach. Learn.*, vol. 30, pp. 3, Jun. 2013.
- [34] S. Ioffe and C. Szegedy, "Batch normalization: Accelerating deep network training by reducing internal covariate shift," in *Proc. Int. Conf. Mach. Learn.*, pp. 448-456, Jul. 2015.
- [35] K. He, X. Zhang, S. Ren, and J. Sun, "Deep residual learning for image recognition," in *Proc. IEEE Int. Conf. Comput. Vis. Pattern Recognit.*, pp. 770-778, Jun. 2016.
- [36] X. Glorot and Y. Bengio, "Understanding the difficulty of training deep feedforward neural networks," in *Proc. Conf. Artificial Intelligence and Statistics*, vol. 9, pp. 249-256, May. 2010.
- [37] D. P. Kingma and J. Ba, "Adam: A method for stochastic optimization," arXiv preprint arXiv:1412.6980, Dec. 2014.
- [38] A. Paszke et al., "Pytorch: An imperative style, high-performance deep learning library," in *Proc. Adv. Neural Inf. Process. Syst.*, vol. 32, pp. 8026-8037, Dec. 2019.
- [39] J. Zbontar et al., "fastMRI: An open dataset and benchmarks for accelerated MRI," arXiv preprint arXiv:1811.08839, Nov. 2018.
- [40] M. Uecker et al., "ESPIRiT—an eigenvalue approach to autocalibrating parallel MRI: where SENSE meets GRAPPA," *Magn. Reson. Med.*, vol. 71, no. 3, pp. 990-1001, May. 2014.
- [41] S. M. Smith, "Fast robust automated brain extraction," *Hum. brain map.*, vol. 17, no. 3, pp. 143-155, Sep. 2002.
- [42] S. Laine, T. Karras, J. Lehtinen, and T. Aila, "High-quality self-supervised deep image denoising," in *Proc. Adv. Neural Inf. Process. Syst.*, vol. 32, pp. 6970-6980, Dec. 2019.
- [43] T. W. Redpath, "Noise correlation in multicoil receiver systems," *Magn. Reson. Med.*, vol. 24, no. 1, pp. 85-89, Mar. 1992.
- [44] P. B. Roemer, W. A. Edelstein, C. E. Hayes, S. P. Souza, and O. M. Mueller, "The NMR phased array," *Magn. Reson. Med.*, vol. 16, no. 2, pp. 192-225, Nov. 1990.

- [45] O. Ronneberger, P. Fischer, and T. Brox, "U-net: Convolutional networks for biomedical image segmentation," in *Proc. Int. Conf. Med. Image Comput. Comput.-Assist. Intervent.*, vol. 9351, pp. 234-241, Nov. 2015.
- [46] D. Dereniowski and M. Kubale, "Cholesky factorization of matrices in parallel and ranking of graphs," in *Int. Conf. Parallel Process. Appl. Math.*, pp. 985-992. Sep. 2004.